Published in final edited form as:
Neuroimage. 2013 November 15; 82: . doi:10.1016/j.neuroimage.2013.05.063.

Spatial–temporal atlas of human fetal brain development during the early second trimester

Jinfeng Zhan[a,b], **Ivo D. Dinov**[b], **Junning Li**[b], **Zhonghe Zhang**[a,c], **Sam Hobel**[b], **Yonggang Shi**[b], **Xiangtao Lin**[a,d], **Alen Zamanyan**[b], **Lei Feng**[a], **Gaojun Teng**[e], **Fang Fang**[e], **Yuchun Tang**[a], **Fengchao Zang**[e], **Arthur W. Toga**[b,*], and **Shuwei Liu**[a,**]

[a]Research Center for Sectional and Imaging Anatomy, Shandong University School of Medicine, 44 Wen-hua Xi Road, 250012 Jinan, Shandong, China

[b]Laboratory of Neuro Imaging, Department of Neurology, University of California School of Medicine, Los Angeles, CA 90095, USA

[c]Department of Medical Imaging, Provincial Hospital Affiliated to Shandong University, 250021 Jinan, Shandong, China

[d]Department of MRI, Shandong Institute for Medical Imaging, 250021 Jinan, Shandong, China

[e]Department of Radiology, Zhong Da Hospital, Southeast University School of Clinical Medicine, 210009 Nanjing, Jiangsu, China

Abstract

During the second trimester, the human fetal brain undergoes numerous changes that lead to substantial variation in the neonatal in terms of its morphology and tissue types. As fetal MRI is more and more widely used for studying the human brain development during this period, a spatiotemporal atlas becomes necessary for characterizing the dynamic structural changes. In this study, 34 postmortem human fetal brains with gestational ages ranging from 15 to 22 weeks were scanned using 7.0 T MR. We used automated morphometrics, tensor-based morphometry and surface modeling techniques to analyze the data. Spatiotemporal atlases of each week and the overall atlas covering the whole period with high resolution and contrast were created. These atlases were used for the analysis of age-specific shape changes during this period, including development of the cerebral wall, lateral ventricles, Sylvian fissure, and growth direction based on local surface measurements. Our findings indicate that growth of the subplate zone is especially striking and is the main cause for the lamination pattern changes. Changes in the cortex around Sylvian fissure demonstrate that cortical growth may be one of the mechanisms for gyration. Surface deformation mapping, revealed by local shape analysis, indicates that there is global anterior–posterior growth pattern, with frontal and temporal lobes developing relatively quickly during this period. Our results are valuable for understanding the normal brain development trajectories and anatomical characteristics. These week-by-week fetal brain atlases can be used as reference in in vivo studies, and may facilitate the quantification of fetal brain development across space and time.

Keywords

Fetal MRI; Second-trimester; Atlas; Human brain development

*Corresponding author. toga@loni.ucla.edu. **Corresponding author. Fax: +86 531 88382502. liusw@sdu.edu.cn..

Conflict of interest The authors declare no competing financial interests.

Introduction

Human brain development is a complex and varying process. Significant progress toward our understanding of the fetal brain can be made by studying it using advanced magnetic resonance imaging (MRI) techniques. MRI has many advantages in the clinical diagnosis of potential abnormalities during pregnancy, especially for the developing central nervous system (Coakley et al., 2004; Glenn and Barkovich, 2006; Twickler et al., 2003), including high spatial resolution, good tissue contrast, and the ability to collect functional information (Brugger et al., 2006; Prayer et al., 2006; Rutherford et al., 2008). Additionally, the availability of post-acquisition morphometric methods and powerful new software tools enables the study of early fetal brain development and maturation in vivo. For instance, the use of age-specific atlases can significantly improve the results of automated analysis of brain MRI data (Prastawa et al., 2005; Serag et al., 2012; Weisenfeld and Warfield, 2009; Xue et al., 2007; Yoon et al., 2009).

The second trimester commences during the 14th week of pregnancy and extends through the 27th week, and is considered to be a specific window of vulnerability for the fetus (Miranda, 2012). During this period, the enormous rate of neurogenesis and neuronal migration are in overdrive, so relatively minor disruptions may significantly alter the structure and function of the maturing brain. Studies of normal and pathological brain development during this period are critical for our understanding of the causality and the associations between neurological traits and different environmental factors. In clinical settings, fetal MRI is usually performed after the 19th gestational week (GW). Therefore, most fetal MRI studies, including construction of spatial–temporal brain atlases, 3D reconstruction, tissue segmentation etc., are focused on the later period of the second trimester and afterwards (Habas et al., 2010a, 2010b; Perkins et al., 2008; Scott et al., 2011; Serag et al., 2012). However, there are only a few studies focusing on the early second trimester. Two-dimensional (2D) histological atlases of this period have been previously developed (Bayer and Altman, 2005). Recently, a study based on diffusion tensor imaging (DTI) investigated fetal brain development during 13–22 GW by DTI color maps, tractography, and three-dimensional (3D) reconstruction (Huang et al., 2009). The development of age and population-specific brain atlases for the early second trimester will facilitate the quantification of fetal brain development and allow us to understand the normal developmental trajectories and characteristics. However, most current atlasing efforts and resources have limited capabilities for making 3D spatiotemporal atlases of fetal MR structure, which prevents the exploration of anatomical development trajectory using surface modeling or morphometric analysis of fetal brain imaging data.

Neuroimaging during early fetal development is complicated due to the smaller brain-size, poor tissue differentiation, and frequent fetal generic movements (Brugger, 2011). It is difficult to obtain high-quality images showing detailed local anatomy. Nevertheless, postmortem fetal specimens offer advantages in imaging by allowing the use of high-field strength magnets, smaller field of view, reduced slice thickness, and increased acquisition time. Some pioneering studies of 15–36 GW have demonstrated the powerful correspondences between fetal architectonic zones and MRI bioimaging markers (Judas et al., 2005; Kostovic et al., 2002; Rados et al., 2006).

In this study, we used 34 fetal specimens between 15 and 22 GW, which were acquired in a high-field 7.0 T MR scanner. Brain templates for every week of gestation, spanning the entire 8-week period, were established using Advanced Normalization Tools (ANTs) (Avants et al., in press). In addition, cortical surfaces for every subject were extracted, modeled, registered, and their differences analyzed into the common template space. These

week-by-week fetal brain atlases provide a mechanism for quantitative assessment of morphometric brain changes and yield clues to the underlying brain maturation patterns during the early second trimester.

Materials and methods

Data acquisition

The thirty-four postmortem (male and female) fetal specimens of 15–22 weeks GW in this study were partially or totally used to study laminar organization, brain development characteristics at 20th gestational week and cortical folding in our previous publications (Zhang et al., 2010, 2011a, 2011b). They were collected from medically indicated or spontaneous abortions, fetal deaths caused by maternal diseases, stillbirths during abnormal labor, and premature deaths attributed to diseases outside of the brain (such as respiratory disease) in hospitals of Shandong Province, China. The demographic distributions of the specimens are listed in Table 1. The specimens were first examined with ultrasound and 3.0 T MR pre-scanning to exclude those with brain diseases or developmental disorders. The criteria by which a fetus was deemed to be anatomically normal were based on the size of the cerebrum and developmental status of sulci, lateral ventricle, and corpus callosum. Only those that had a morphologically intact central nervous system were included in the study. The GW of the fetuses was estimated on the basis of their crown–rump length, head circumference, foot length, and/or pregnancy records and expressed as weeks from the last menstrual period (Guihard-Costa et al., 2002). All specimens were immersed in 10% formalin for preservation without extracting the brain. The time interval between collection of specimens and scanning was less than 2 months. The intensity distribution on T2 MRI for fetal brain after formalin preservation is corresponding to the in vivo and histological studies (Pugash et al., 2011). This study was conducted based on prior approval from the Internal Review Board of the Ethical Committee at the School of Medicine, Shandong University. The parents' consent to donate the fetal cadaver was obtained before imaging and specimen preparation.

Fetal imaging is performed in a 7.0 T Micro-MRI with a maximum gradient of 360 mT (70/16 PharmaScan, Bruker Biospin GmbH, Germany). Each fetal brain was scanned in situ and was fit into a rat-size body coil with an inner diameter of 60 mm and 2D T2-weighted (T2w) slice images (pixel size 0.19 mm × 0.19 mm or 0.23 mm × 0.23 mm, slice thickness = 0.5 mm) were acquired in the axial plane with respect to the fetal brain. The acquisition parameters were as follows: TR/TE = 12,000/50 ms, matrix = 256 × 256, and NEX = 4.

Data processing

Image preprocessing—The native DICOM imaging data were converted to NIFTI and Analyze formats using FreeSurfer's MRI convert module (Fischl and Dale, 2000). Intensity inhomogeneity correction was applied to all converted data using the N3 algorithm (Sled et al., 1998). Both the data conversion and bias field correction were implemented as Pipeline workflows (Dinov et al., 2009b, 2010, 2011). Our attempts to automatically skull strip the fetal brain volumes using SSMA (Leung, 2011; Leung et al., 2008) and BET (Smith, 2002) were unsuccessful. Manual removal of the non-brain tissue for every individual brain was performed using BrainSuite software (Shattuck and Leahy, 2002). The LPBA protocol[1] was used for manually removing extra cerebral tissue — both cerebellum and brainstem were included (Shattuck et al., 2008).

[1] http://www.loni.ucla.edu/twiki/pub/LPBA/ProtocolSupplements/SkullStrippingProtocol.pdf.

Template building—Optimal template construction function of ANTS (version 1.9) was used (Avants et al., in press). ANTS has been demonstrated to be among the most accurate intensity-based normalization methods among fourteen different methods (Klein et al., 2009). The script *buildtemplateparallel.sh* (Avants and Gee, 2004; Avants et al., 2008) was run for all specimens within each gestational week, using the default settings except for an additional option "−r 1" to turn on rigid-body registration. Following the ANTS recommendations, we used symmetric diffeomorphic mapping (SyN) energy terms, which measure image similarity and diffeomorphism lengths for the diffeomorphic transformations. The ANTS–SyN approach is defined by the minimum shape and appearance distance image. It uses symmetric pair-wise mapping, symmetrically optimizes the two terms in normalization methods (geometry and appearance) across the population and is unbiased; that is, it does not prefer any specific image input by the user or specific guess for the initial template. Instead, the template should be derived completely from the database of *n* images. The procedure first optimizes the mappings with a fixed template, then, optimizes the template appearance with fixed shape and mappings, and, finally, optimizes the template shape. The process then repeats (Fig. 1).

Temporal modeling of anatomical deformations—The growth-related changes in the size and shape of the fetal brain are captured by the components of the affine scaling and the displacement fields estimated during the diffeomorphic registration. For each symmetric pairwise mapping, Affine and Warp transformation files were computed for each subject. Using the ANTS script *ComposeMultiTransform.sh*, the affine and warp files were made into one deformation file, and the two deformation files of the two steps during the template build were also made into one total deformation field. This total deformation field was used to calculate the Jacobian (with ANTS script: *ANTSJacobian.sh*), which reflected the non-linear deformation field of temporal changes at each voxel location. Using FSLStats module in LONI Pipeline (Dinov et al., 2009a), we obtain the mean and standard deviation (as univariate measures) of the Jacobian field at each voxel location.

Global measurement and surface analysis—Using the skull-stripped brain volumes for each subject, BrainSuite's surface extraction tool (Shattuck and Leahy, 2000) was used to obtain topologically correct cortical surface models (triangulated 2-manifolds). For each cortex, 6 complementary global shape metrics were computed using LONI ShapeTools pipeline library (Joshi et al., 2012) — surface area, fractal dimension, shape index, curvedness, shape-index and volume. These were added to the subject demographics as derived imaging biomarkers, along with the overall (global) Jacobian value obtained from linearly registering the template to each individual subject's brain.

The local shape analysis (LSA) pipeline workflow (Dinov et al., 2011) was employed to obtain local shape metrics (displacement-field, radial-distance), per vertex in the triangulated surface representations. The displacement field (Brun et al., 2011; Lepore et al., 2008) and the radial distance (Hua et al., 2011b; Sundar et al., 2003) measures were computed by surface registration of the template cortical model to each individual cortical surface using a diffeomorphic algorithm (Joshi et al., 2012). The displacement feature is computed by applying a (volume-preserving) rigid transformation spatially normalizing each shape to the population-wide mean shape. In placing each surface into the template's space, the magnitude of the displacement field is computed at each vertex point on the surface. The radial distance, on the other hand, measures the distance from each surface point to the central core of the shape (point of gravitational balance). This metric index captures local expansions or contractions of the developing cortical surface. These two local shape measures were used as covariates to generate brain maps representing the associations between derived shape morphometric and GW at each cortical location. The captured surface development patterns will be helpful to discover the growth direction of fetal brain.

The growth direction specifies the surface that is changing (e.g. anterior aspect of the brain) which may be different from the growth in an orthogonal direction (e.g. A–P axis).

Direct computation of mean curvature on triangular meshes depends heavily on mesh quality and can result in noisy results. For the robust estimation of mean curvature on surfaces, we used the implicit representation of surfaces as *signed distance functions* defied on *regular* grids (Osher and Sethian, 1988), which makes the estimation independent of mesh quality. To convert the triangular mesh representation to implicit representations, we used the fast marching algorithm (Sethian, 1996) to compute the signed distance function. Numerical schemes on Euclidean spaces can then be used to compute the mean curvature on the surface (Osher and Sethian, 1988).

Tensor based morphometry (TBM)—Tensor-based morphometry (TBM) (Hua et al., 2008; Leow et al., 2006) is a method enabling the mapping of structural changes between groups in time or space to identify anatomical differences using 3D non-linear volumetric warping. For instance, TBM analysis may be employed to investigate structural brain changes due to prenatal exposure to methamphetamine (Sowell et al., 2010), alcohol exposure (Paniagua et al., 2011), traumatic brain injury (Kim et al., 2008), or voxel-wise genome-wide association study (Stein et al., 2010). Regional structural differences of deformation fields (tensors) are represented as TBM maps and identify the relative positions of different brain structures. The first step in TBM analysis is the non-affine spatial normalization of all structural images into a common anatomical space. This facilitates the localized quantitative characterization of the population differences using 3 × 3 Jacobian matrices representing the magnitude of the gradient of the displacement vector fields. After generating a brain template for each GW, each subject's brain is warped to the corresponding template and the determinant of the Jacobian of this transformation is computed. At each voxel, this Jacobian map represents a univariate measure of relative volume change caused by the spatial deformation (Hua et al., 2011a). The Jacobian determinants are interpreted as volume loss ($\det|J| < 1$), volume gain ($\det|J| > 1$), or no change ($\det|J| = 1$) (Brun et al., 2011).

Statistical analysis

The general linear model (Calabrese et al., 2011; Che et al., 2009a, 2009b) was used to study the associations between subject metadata (e.g., demographics and GW) and derived biomedical imaging markers (e.g., radial-distance, Jacobians). A prior false-positive rate of $\alpha = 0.05$ was used to determine significant effects. False discovery rate (FDR) (Benjamini and Hochberg, 1995; Che et al., 2009b) was employed to correct the false-positive error rate due to multiple testing. The computational libraries of the Statistics Online Computational Resources (SOCR) (Che et al., 2009b; Christou and Dinov, 2011) wrapped as Pipeline modules (Dinov et al., 2010) were used for some exploratory data analysis and for computing various image and shape-based statistics. The SOCR multivariate statistics module generates four types of results. These include: B: beta, effect-size of specific covariate (X, e.g., GW) on the response variable (Y, e.g., Jacobian); T: the T-statistics represents a standardized version of the Beta effect size (degrees-of-freedom depend on the sample-sizes); R: partial correlation (ρ) map between a specific covariate (X) and the response variable (Y); and P: probability value corresponding to the T-statistical map, which quantifies the strength of the evidence to reject the Null-hypothesis (H_o: $B = 0$ vs. H_a: $B \neq 0$).

Results

Global growth trajectories

To obtain the global growth trajectories, a simple regression analysis was performed on the whole brain area and volume relative to GW. The whole brain increased in volume by approximately 4-fold from 15 to 22 GW and about 2.5-fold in area. Our results showed the fast growth trajectories of brain area and volume is fitted well by linear model (with R^2 value = 0.919 and 0.940 respectively) (Fig. 2).

Spatiotemporal atlas

To construct the Fetal Brain Atlas of the early second trimester we first computed the atlas templates for every week from 15 to 22. To minimize the bias effects of different demographic distributions, as there were different numbers of cases within each week, the aggregated general template was built from these weekly templates, rather than by pooling all subjects together (Fig. 3). The atlas is publicly available to the entire community via the LONI Atlases download site (http://www.loni.ucla.edu/Atlases/Atlas_Detail.jsp?atlas_id=22).

For each weekly template, the surface models were generated as genus-zero 3D triangulated manifolds (Lai and Chan, 2011). The differences in shape, form and size of these weekly surface models illustrate the development process of fetal brain (Fig. 4). In the 15th week, we can still grasp some trails of neural folding in the early stages. By the 22nd week, the brain surface still looks smooth, but the Sylvian fissure becomes more typical and the whole brain's general shape looks more mature.

Cerebral wall

A number of structures can be recognized on the template. Nuclear structures such as thalamus, caudate nucleus and putamen, displayed moderate intensity. Four layers of the cerebral wall can be recognized, from ventricular to the pial surface, these layers are: (1) ventricular zone (VZ) with hypointense signal on T2 images, which corresponds to the high cell-packing density. Ganglionic eminence represents a localized thickening of ventricular zone, which is most obvious in the temporal and occipital horn of lateral ventricle; (2) intermediate zone (IZ) with moderate MRI signal intensity, which encompasses fetal white matter; (3) subplate zone (SP) with hyperintense signal, which corresponds to heterogeneous population of neurons with abundant extracellular matrix. Subplate thickness varies in different locations of the brain. It is thicker in the lateral surface of frontal and temporal lobes and the dorsal surface of the parietal lobe, but thinner in the insular gyrus, which lies on the medial surface of frontal to the occipital lobes. (4) Cortical plate (CP) with hypointense signal, which corresponds to tightly packed columns of cells. Subplate zone occupies almost the entire outer half of the fetal cerebral wall, while IZ occupies deep periventricular regions (Fig. 5).

For the evaluation of temporal models of anatomical changes, we regressed the TBM/Jacobian maps on GW. 3D spatial maps of the FDR-corrected P-values (FDR-P), effect-sizes (B) and correlations (T and R) are shown in Fig. 6. These maps represent the locations of significant GW-effects on the magnitude of the Jacobian maps, based on a general linear model. Both B coefficients and P-values indicated that large portions of the entire brain showed significant growth.

Nearly the entire cerebral wall grows with significant correlations, except for parts of ventricular zone and intermediate zone in the frontal and occipital lobes. The subplate is hyperintense beneath the cortical plate on T2 MR images and can be easily visualized due to

its abundance of the hydrophilic extracellular matrix (Judas et al., 2003; Kostovic and Judas, 2002). Compared with other layers, the subplate zone and part of cortical plate adjacent to the SP where migration and synaptogenesis happen, show more significant correlation with GW and a bigger growth rate. That means steady and consistent temporal shape changes happen in the SP during this period. Regional developmental differences could be found within the subplate zone as well. The subplate zone in the lateral surface of frontal and temporal lobes and the dorsal surface of the parietal lobe show a higher correlation and bigger growth rate (Fig. 6). However, the ventricular zone (including ganglionic eminence), which is the source of neurons during the early fetal life, does not show significant changes and neither does the intermediate zone in the frontal and occipital lobes. Subcortex nuclei and thalamus have moderate growth rates and correlations with GW.

Lateral ventricles

The lateral ventricles are the dominant structure early in the second trimester. In our results, lateral ventricles in the frontal and parietal lobes show negative B, T and R values after applying FDR-P, which implies local volume contractions. The parasagittal view is chosen to display the most obvious shrinking areas (Fig. 7).

Sylvian fissure

Curvature is displayed in the lateral surface of every week's templates and the overall template, which can give us a general view for the appearance and process of sulcation (Fig. 8). From the lateral view, the Sylvian fissure is the most obvious sulcus that we can detect through all the periods in our studies. In the early gestation weeks, the Sylvian fissure is widely open with an obtuse angle and appears as a shallow fossa. Subsequently, it becomes deeper and longer. By the 19th gestational week, the circular sulcus appears in the superior border of the Sylvian fissure. The circular sulcus extends and then curves around to form a circular pattern. As the frontal lobe develops, the circular sulcus will gradually lose its circular shape and finally join the Sylvian fissure as a single deep fissure (Chi et al., 1977).

The cortex around the Sylvian fissure, especially on the frontal and parietal lobes, has a higher growth rate and more significant R and T values (Fig. 9). We can deduce that the faster growth of the cortex contributes to the modeling of the Sylvian fissure, causing it to change from being open and shallow to being deep and narrow.

Growth direction

For each GW the local displacement-field and radial-distance measures were first mapped onto the template surface. Independent statistical comparisons were then carried out at each vertex using SOCR tools and the resulting statistical maps were projected onto the average surface. The most striking and significant changes in displacement-field were observed in the anterior region of temporal lobe. In the inferior–posterior surface of temporal lobe, negative B and T values are dominant (Fig. 10). These local displacement-field changes directly measure the morphometric changes in the temporal lobe, which transforms from being relatively short and wide in the 15 GW period, to being long and narrow by 22 GW. For the entire cortical surface, there are more vertices with positive B and T values in both the anterior and posterior areas, however more negative ones superiorly and inferiorly. For the radial-distance metric, only positive B and T values were observed. This implies that every vertex on the surface undergoes outward movement and the surface as a whole is radially expanding from 15 to 22 GW (Fig. 11). However, vertices in the anterior surface of the frontal lobe, the temporal lobes and the posterior surface of the occipital lobe have higher B values and more significant corresponding T values. This implies that the brain shape extends in both the anterior and posterior directions during 15–22 weeks of gestation. In particular, vertices in the anterior frontal and temporal areas show more dramatic

expansion. Thus, the brain undergoes a more profound anterior development specifically during this period.

Discussion

Second trimester represents the development peak for the human fetal telencephalon (Judaš, 2011). We modeled the global growth trajectories of male and female human fetal brain's volume and area between 15 and 22 GW, and presented a spatiotemporal template of the fetal brain with temporal models of MR intensity and shape changes. Voxel-wise linear modeling allows us to capture the spatial variation of brain structures over time. Three-dimensional reconstruction demonstrates the morphological changes of fetal brain during the early second trimester. Because 1.5 T MRI is routinely used in clinic and performed often after 19 GW, the earliest fetal templates based on the in vivo MRI data and population registration are ranging from 20.57 to 22.86 weeks (Habas et al., 2010b) and 20.57–24.71 weeks (Habas et al., 2010a). Because of the relatively poor resolution of fetal MRI scans in vivo, only four main tissue types with different tissue contrasts can be distinguished; they are defined as developing cortical gray matter, developing white matter, germinal matrix and ventricles. However these tissue types can't represent all the real anatomical structures. For example, the developing white matter includes subplate zone, intermediate zone and some other subcortical nuclei. In our study, the use of 7.0 T MR images allows us to build templates with much better tissue contrast. Not only the main subcortex structures, such as basal ganglia nuclei, but also the laminar organization of cerebral wall can be identified with relatively clear boundaries. Based on the template, we performed parametric modeling of changes in MR shape of the developing fetal brain. This method was also used in a previous in vivo study to capture the main growth pattern during 20.57–24.71 GW (Habas et al., 2010a). Although additional features such as gender, head circumference or abortion reasons could also be considered, we used gestational week as the only independent variable for this initial work. Linear temporal model provides a good description of development patterns and allows us to represent both contraction and expansion in different regions of the fetal brain.

Fetal cerebral wall is formed by architectonic zones that represent a spatial framework for specific histogenetic events, such as neuronal proliferation, migration, and establishment of cortical neuronal connections. The layered appearance of the fetal cerebral wall was already observed in early MRI studies (Felderhoff-Mueser et al., 1999; Garel et al., 2001; Girard et al., 1995; Lan et al., 2000; Sbarbati et al., 1998). Our study demonstrates that 7.0 T MRI provides excellent image quality for studying fetal brains that can characterize typical fetal lamination pattern of different cortical layers during the early second trimester. A previous study using Nissl-stain enabled the delineation of seven laminar compartments within the cerebral wall: ventricular zone, periventricular zone, subventricular zone, intermediate zone, subplate zone, cortical plate and marginal zone (Kostovic et al., 2002). The spatiotemporal microstructural changes of cerebral wall in the postmortem fetal brain from 13 to 21 GW were also quantitatively characterized in a previous DTI study. It was indicated that three layers can be clearly differentiated in most regions of the cerebral wall in the FA (fractional anisotropy) map; they are the cortical plate (with marginal zone), subplate zone, and an inner layer (including intermediate zone, subventricular zone, and ventricular zone) (Huang et al., in press). In this template, four laminar compartments could be clearly delineated: ventricular zone, intermediate zone, subplate zone, and cortical plate. Regarding the similar content of adjacent layers, it is thought that, in the template we built, the ventricular zone includes the periventricular zone, the intermediate zone includes the subventricular zone, and cortical plate includes the marginal zone. The subplate zone shows the most obvious growth pattern, which implies that changes in the lamination pattern of the cerebral wall are predominantly caused by changes in the subplate zone. This result confirms a previous

observation study based on MRI and histology (Kostovic et al., 2002). Furthermore, another study quantitatively analyzed the volume and thickness of subplate zone and found that the subplate showed significant development pattern from 18 to 24 gestational weeks (Corbett-Detig et al., 2011). The subplate zone is the most prominent transient compartment of the cerebral wall. Numerous functions have been attributed to the subplate zone, including the accumulation and waiting area for axons predetermined to synapse in the developing cortex, while their target cells are still being generated in the ventricular zone. They then migrate through the intermediate and subplate zones to the cortical plate. Axonal connections will be established when the axons can reach the appropriate target cells in the cortical plate. This is important in the development of the thalamocortical and other cortical afferent connections (Sur and Rubenstein, 2005). Thus, one can expect that as the cortical afferents accumulate and wait in the subplate zone, the thickness of subplate zone will become steadily bigger, which is confirmed by our spatio-temporal correlation results. We can infer that more migration and accumulation but less synaptogenesis happens in the subplate zone during 15–22 weeks. After 34–36 GW, as axons move from the subplate zone to synapse in the cortical plate, the subplate zone disappears gradually (Kostovic and Jovanov-Milosevic, 2008). Regional differences in the development and thickness of the subplate zone are also apparent. These kinds of regionally specific growth patterns were also found in a subplate thickness study focusing on 18–22 GW (Corbett-Detig et al., 2011). In our template, the subplate zone in the lateral surface of the frontal and temporal lobes shows greater thickness and has better correlation with GW and higher growth rate. Moreover, the subplate zone in these areas persists longest (Rutherford et al., 2008). The primary sensory signals of vision, audition and touch pass through the thalamus en route to the cortex in the parts of the frontal, parietal and temporal lobes. That means there will be more thalamocortical afferents waiting in the subplate zone, which causes greater thickness and growth rate of the subplate zone located in these areas, as described in our results. The lateral ventricles appear more prominent in early gestation due to the thin brain parenchyma relative to ventricular size at early gestational ages. Our results demonstrate that as gestation progresses, the size of the ventricles decreases. One possible reason is that the thickness of the cortical mantle increases relative to the ventricles. As the basal ganglia enlarge, the ventricles display their typical shape (Prayer et al., 2006). Abnormal width of the lateral ventricles may be the first sign of developmental anomalies (Prayer et al., 2011). For example, isolated mild ventriculomegaly (IMVM) is the most common brain abnormality on the prenatal ultrasound diagnosis and its potential changes of ventricular have been specified in an MRI study (Scott et al., 2012). A recent study applied multi-atlas, multi-shape automatic segmentation method to shape segmentation of normal, dilated, or fused lateral ventricles for quantitative analysis of ventriculomegaly (VM) in the GW range of 19 to 39 weeks, and propose biomarkers for the detection of VM (Gholipour et al., 2012). Therefore, modeling the normal development of the lateral ventricle will be valuable for clinical evaluation and early diagnosis.

Cortical gyration occurs relatively late in fetal development. Early in the second trimester, the cortex is a smooth, lissencephalic surface, with only one shallow Sylvian fossa. Afterwards, the Sylvian fossa gradually becomes more complex and morphs into a longer and deeper fissure. Not until the third trimester will there be rapid development of gyri and sulci (Pugash et al., 2011). So far, several hypotheses have been put forward to explain the mechanisms of sulcal formation during development, including sulcation resulting from cortical growth (Toro and Burnod, 2005), variable growth between inner and outer cortical layers, and mechanical pulling by white matter fibers connecting cortical areas (Hilgetag and Barbas, 2005; Van Essen, 1997). Our results demonstrate that locally the Sylvian fissure cortex shows faster growth rate than other areas. One recent vivo study based on direction-specific TBM method also found that the voxels underlying the Sylvian fissure show significant changes with age, and the combination growth acceleration along the right–left axis and deceleration along superior–inferior axis at the superior aspect of the temporal lobe

results in deepening and closing of the Sylvian fissure (Rajagopalan et al., 2012). Together with our finding in the early development of Sylvian fissure, we can conclude that local cortical growth may be one important mechanism to explain the formation of cortical folding. The parts of the cortex with higher growth rate in our results relate to the Sylvian fissure, as well as those that will become the future parts of the sensory and motor cortex. This confirms a previous finding that gyral development is most rapid in areas of the sensory pathway (Barkovich et al., 1988).

By analyzing changes of displacement-field and radial-distance in the local surface, we found an anterior–posterior bidirectional globalshape growth pattern of the human fetal brain during 15–22 GW. A previous study reports that the corpus callosum also shows a similar growth pattern (Huang et al., 2009). This result explains the developmental path of the fetal brain shape from a sphere to an oval by gradually morphing into its mature shape. Thus, antero-posterior diameter of the fetal brain has a tendency to increase. This implies that the medial regions of brain develop early on or before 15 GW. After 15 GW, the anterior of the frontal and temporal lobes shows more significant and faster growth development. Since both prefrontal cortex (PFC) and anterior temporal lobe (ATL) with dramatic expansion are brain regions of complex functions (Bell et al., 2011; Yang and Raine, 2009), this kind of growth direction patterns may be related to brain function development. But extra information, obtained through extending the study age range or through combining multimodality methods, is still necessary to confirm this. We built a spatiotemporal template ranging from 15 to 22 gestational weeks. By reconstructing every week's template in four space-time dimensions, we displayed their morphological changes. After registration, we analyzed spatial and developmental variations of cerebral wall, lateral ventricles, Sylvian fissure and local measurements of displacement-field and radial-distance. We modeled some characteristics of development during the early second trimester. The use of high field MRI allows us to obtain good quality images and better characterize the 3D architecture of the developing brain. Not only did our results correspond well to past histological studies, but they may also be helpful for understanding and analyzing the fetal brain development and relative disorders in future studies. We are currently expanding the atlas to include tissue segmentation and region parcellation. With the help of the template we already have, tissue probability maps will be generated and then used to initialize automatic tissue delineation in new MR images.

Acknowledgments

This study was supported by the National Natural Science Foundation of China (No. 31071050; No. 81001223); in part by the following National Institutes of Health grants NIA P 50 AG16570, NIBIB EB01651, NLM LM05639, NCRR RR019771, NIMH R01 MH071940, NIBIB 9P41EB015922-15, NCRR 2-P41-RR-013642-15, NCRR U54 RR021813, U24-RR025736, and U24-RR021992; Graduate Students Innovation Funds of Shandong University (No. 21300070613236); Doctoral Foundation of Shandong Province (Nos. BS2010YY042, BS2010YY048, BS2012YY009) and Special Funds for Postdoctoral Innovative Projects of Shandong Province (No. 201002024).

References

Avants B, Gee JC. Geodesic estimation for large deformation anatomical shape averaging and interpolation. Neuroimage. 2004; 23(Suppl. 1):S139–S150. [PubMed: 15501083]

Avants BB, Epstein CL, Grossman M, Gee JC. Symmetric diffeomorphic image registration with cross-correlation: evaluating automated labeling of elderly and neurodegenerative brain. Med. Image Anal. 2008; 12:26–41. [PubMed: 17659998]

Avants BB, Tustison N, Song G. Advanced Normalization Tools (ANTS). Insight J. 2009 (in press).

Barkovich AJ, Kjos BO, Jackson DE Jr. Norman D. Normal maturation of the neonatal and infant brain: MR imaging at 1.5 T. Radiology. 1988; 166:173–180. [PubMed: 3336675]

Bayer, S.; Altman, J. The Human Brain during the Second Trimester (Atlas of the Human Central Nervous System Development). CRC Press, Indianapolis; 2005.

Bell B, Lin JJ, Seidenberg M, Hermann B. The neurobiology of cognitive disorders in temporal lobe epilepsy. Nat. Rev. Neurol. 2011; 7:154–164. [PubMed: 21304484]

Benjamini Y, Hochberg Y. Controlling the false discovery rate: a practical and powerful approach to multiple testing. R. Stat. Soc. 1995; 57:289–300.

Brugger, PC. Methods of fetal MRI. In: Prayer, D., editor. Fetal MRI. Springer; Berlin Heidelberg: 2011. p. 65-80.

Brugger PC, Stuhr F, Lindner C, Prayer D. Methods of fetal MR: beyond T2-weighted imaging. Eur. J. Radiol. 2006; 57:172–181. [PubMed: 16377112]

Brun CC, Lepore N, Pennec X, Chou Y, Lee AD, de Zubicaray G, McMahon K, Wright MJ, Gee JC, Thompson PM. A non-conservative Lagrangian framework for statistical fluid registration — SAFIRA. IEEE Trans. Med. Imaging. 2011:1–1.

Calabrese A, Schumacher JW, Schneider DM, Paninski L, Woolley SMN. A generalized linear model for estimating spectrotemporal receptive fields from responses to natural sounds. PLoS One. 2011; 6:e16104. [PubMed: 21264310]

Che A, Cui J, Dinov I. SOCR analyses — an instructional Java web-based statistical analysis toolkit. JOLT. 2009a; 5:1–19. [PubMed: 21546994]

Che A, Cui J, Dinov I. SOCR analyses: implementation and demonstration of a new graphical statistics educational toolkit. JSS. 2009b; 30:1–19. [PubMed: 21666874]

Chi JG, Dooling EC, Gilles FH. Gyral development of the human brain. Ann. Neurol. 1977; 1:86–93. [PubMed: 560818]

Christou N, Dinov I. Confidence interval based parameter estimation — a new SOCR applet and activity. PLoS One. 2011; 6(5):e19178. [PubMed: 21655319]

Coakley FV, Glenn OA, Qayyum A, Barkovich AJ, Goldstein R, Filly RA. Fetal MRI: a developing technique for the developing patient. AJR Am. J. Roentgenol. 2004; 182:243–252. [PubMed: 14684546]

Corbett-Detig J, Habas PA, Scott JA, Kim K, Rajagopalan V, McQuillen PS, Barkovich AJ, Glenn OA, Studholme C. 3D global and regional patterns of human fetal subplate growth determined in utero. Brain Struct. Funct. 2011; 215:255–263.

Dinov I, Van Horn J, Lozev K, Magsipoc R, Petrosyan P, Liu Z, MacKenzie-Graham A, Eggert P, Parker D, Toga A. Efficient, distributed and interactive neuroimaging data analysis using the LONI pipeline. Front. Neuroinform. 2009a; 3:1–10. [PubMed: 19198661]

Dinov ID, Van Horn JD, Lozev KM, Magsipoc R, Petrosyan P, Liu Z, Mackenzie-Graham A, Eggert P, Parker DS, Toga AW. Efficient, distributed and interactive neuroimaging data analysis using the LONI pipeline. Front. Neuroinform. 2009b; 3:22. [PubMed: 19649168]

Dinov I, Lozev K, Petrosyan P, Liu Z, Eggert P, Pierce J, Zamanyan A, Chakrapani S, Van Horn J, Parker D, Magsipoc R, Leung K, Gutman B, Woods R, Toga A. Neuroimaging study designs, computational analyses and data provenance using the LONI pipeline. PLoS One. 2010; 5:e13070. http://dx.doi.org/10.1371/journal.pone.0013070. [PubMed: 20927408]

Dinov I, Torri F, Macciardi F, Petrosyan P, Liu Z, Zamanyan A, Eggert P, Pierce J, Genco A, Knowles J, Clark A, Van Horn J, Ames J, Kesselman C, Toga A. Applications of the pipeline environment for visual informatics and genomics computations. BMC Bioinformatics. 2011; 12:304. [PubMed: 21791102]

Felderhoff-Mueser U, Rutherford MA, Squier WV, Cox P, Maalouf EF, Counsell SJ, Bydder GM, Edwards AD. Relationship between MR imaging and histopathologic findings of the brain in extremely sick preterm infants. AJNR Am. J. Neuroradiol. 1999; 20:1349–1357. [PubMed: 10472997]

Fischl B, Dale AM. Measuring the thickness of the human cerebral cortex from magnetic resonance images. Proc. Natl. Acad. Sci. U. S. A. 2000; 97:11050–11055. [PubMed: 10984517]

Garel C, Chantrel E, Brisse H, Elmaleh M, Luton D, Oury JF, Sebag G, Hassan M. Fetal cerebral cortex: normal gestational landmarks identified using prenatal MR imaging. AJNR Am. J. Neuroradiol. 2001; 22:184–189. [PubMed: 11158907]

Gholipour A, Akhondi-Asl A, Estroff JA, Warfield SK. Multi-atlas multi-shape segmentation of fetal brain MRI for volumetric and morphometric analysis of ventriculomegaly. Neuroimage. 2012; 60:1819–1831. [PubMed: 22500924]

Girard N, Raybaud C, Poncet M. In vivo MR study of brain maturation in normal fetuses. AJNR Am. J. Neuroradiol. 1995; 16:407–413. [PubMed: 7726092]

Glenn OA, Barkovich J. Magnetic resonance imaging of the fetal brain and spine: an increasingly important tool in prenatal diagnosis: part 2. AJNR Am. J. Neuroradiol. 2006; 27:1807–1814. [PubMed: 17032846]

Guihard-Costa AM, Menez F, Delezoide AL. Organ weights in human fetuses after formalin fixation: standards by gestational age and body weight. Pediatr. Dev. Pathol. 2002; 5:559–578. [PubMed: 12399830]

Habas PA, Kim K, Corbett-Detig JM, Rousseau F, Glenn OA, Barkovich AJ, Studholme C. A spatiotemporal atlas of MR intensity, tissue probability and shape of the fetal brain with application to segmentation. Neuroimage. 2010a; 53:460–470. [PubMed: 20600970]

Habas PA, Kim K, Rousseau F, Glenn OA, Barkovich AJ, Studholme C. Atlas-based segmentation of developing tissues in the human brain with quantitative validation in young fetuses. Hum. Brain Mapp. 2010b; 31:1348–1358. [PubMed: 20108226]

Hilgetag CC, Barbas H. Developmental mechanics of the primate cerebral cortex. Anat. Embryol. (Berl.). 2005; 210:411–417. [PubMed: 16175385]

Hua X, Leow AD, Lee S, Klunder AD, Toga AW, Lepore N, Chou YY, Brun C, Chiang MC, Barysheva M. 3D characterization of brain atrophy in Alzheimer's disease and mild cognitive impairment using tensor-based morphometry. Neuroimage. 2008; 41:19–34. [PubMed: 18378167]

Hua X, Gutman B, Boyle C, Rajagopalan P, Leow AD, Yanovsky I, Kumar AR, Toga AW, Jack CR Jr. Schuff N. Accurate measurement of brain changes in longitudinal MRI scans using tensor-based morphometry. Neuroimage. 2011a; 57(1):5–14. [PubMed: 21320612]

Hua X, Thompson PM, Leow AD, Madsen SK, Caplan R, Alger JR, O'Neill J, Joshi K, Smalley SL, Toga AW. Brain growth rate abnormalities visualized in adolescents with autism. Hum. Brain Mapp. 2011b; 34(2):425–436. [PubMed: 22021093]

Huang H, Xue R, Zhang J, Ren T, Richards LJ, Yarowsky P, Miller MI, Mori S. Anatomical characterization of human fetal brain development with diffusion tensor magnetic resonance imaging. J. Neurosci. 2009; 29:4263–4273. [PubMed: 19339620]

Huang H, Jeon T, Sedmak G, Pletikos M, Vasung L, Xu X, Yarowsky P, Richards LJ, Kostovic I, Sestan N, Mori S. Coupling diffusion imaging with histological and gene expression analysis to examine the dynamics of cortical areas across the fetal period of human brain development. Cereb. Cortex. 2012 (in press).

Joshi S, Cabeen R, Joshi A, Sun B, Dinov I, Narr K, Toga A, Woods R. Diffeomorphic sulcal shape analysis on the cortex. IEEE Trans. Med. Imaging. 2012:1–1. [PubMed: 21768046]

Judaš, M. Prenatal development of the human fetal telencephalon. In: Prayer, D., editor. Fetal MRI. Springer; Berlin Heidelberg: 2011. p. 81-146.

Judas M, Milosevic NJ, Rasin MR, Heffer-Lauc M, Kostovic I. Complex patterns and simple architects: molecular guidance cues for developing axonal pathways in the telencephalon. Prog. Mol. Subcell. Biol. 2003; 32:1–32. [PubMed: 12827969]

Judas M, Rados M, Jovanov-Milosevic N, Hrabac P, Stern-Padovan R, Kostovic I. Structural, immunocytochemical, and MR imaging properties of periventricular crossroads of growing cortical pathways in preterm infants. AJNR Am. J. Neuroradiol. 2005; 26:2671–2684. [PubMed: 16286422]

Kim J, Avants B, Patel S, Whyte J, Coslett BH, Pluta J, Detre JA, Gee JC. Structural consequences of diffuse traumatic brain injury: a large deformation tensor-based morphometry study. Neuroimage. 2008; 39:1014–1026. [PubMed: 17999940]

Klein A, Andersson J, Ardekani BA, Ashburner J, Avants B, Chiang MC, Christensen GE, Collins DL, Gee J, Hellier P, Song JH, Jenkinson M, Lepage C, Rueckert D, Thompson P, Vercauteren T, Woods RP, Mann JJ, Parsey RV. Evaluation of 14 nonlinear deformation algorithms applied to human brain MRI registration. Neuroimage. 2009; 46:786–802. [PubMed: 19195496]

Kostovic I, Jovanov-Milosevic N. Subplate zone of the human brain: historical perspective and new concepts. Coll. Antropol. 2008; 32(Suppl. 1):3–8. [PubMed: 18405051]

Kostovic I, Judas M. Correlation between the sequential ingrowth of afferents and transient patterns of cortical lamination in preterm infants. Anat. Rec. 2002; 267:1–6. [PubMed: 11984786]

Kostovic I, Judas M, Rados M, Hrabac P. Laminar organization of the human fetal cerebrum revealed by histochemical markers and magnetic resonance imaging. Cereb. Cortex. 2002; 12:536–544. [PubMed: 11950771]

Lai R, Chan TF. A framework for intrinsic image processing on surfaces. Comput. Vis. Image Underst. 2011; 115:1647–1661.

Lan LM, Yamashita Y, Tang Y, Sugahara T, Takahashi M, Ohba T, Okamura H. Normal fetal brain development: MR imaging with a half-Fourier rapid acquisition with relaxation enhancement sequence. Radiology. 2000; 215:205–210. [PubMed: 10751488]

Leow AD, Klunder AD, Jack CR Jr. Toga AW, Dale AM, Bernstein MA, Britson PJ, Gunter JL, Ward CP, Whitwell JL. Longitudinal stability of MRI for mapping brain change using tensor-based morphometry. Neuroimage. 2006; 31:627–640. [PubMed: 16480900]

Lepore N, Brun C, Chou YY, Chiang MCA, Dutton RA, Hayashi KM, Luders EA, Lopez OL, Aizenstein HJ, Toga AW, Becker JT, Thompson PM. Generalized tensor-based morphometry of HIV/AIDS using multivariate statistics on deformation tensors. IEEE Trans. Med. Imaging. 2008; 27:129–141. [PubMed: 18270068]

Leung, KTK. Principal Ranking Meta-Algorithms. University of California; Los Angeles: 2011.

Leung, K.; Parker, DS.; Cunha, A.; Dinov, ID.; Toga, AW. SSDBM. Springer-Verlag; 2008. IRMA: an Image Registration Meta-Algorithm — evaluating alternative algorithms with multiple metrics. 2008

Miranda RC. MicroRNAs and fetal brain development: implications for ethanol teratology during the second trimester period of neurogenesis. Front. Genet. 2012; 3:77. [PubMed: 22623924]

Osher S, Sethian JA. Fronts propagating with curvature-dependent speed: algorithms based on Hamilton–Jacobi formulations. J. Comput. Phys. 1988; 79:12–49.

Paniagua, B.; Ehlers, C.; Crews, F.; Budin, F.; Larson, G.; Styner, M.; Oguz, I. Using tensor-based morphometry to detect structural brain abnormalities in rats with adolescent intermittent alcohol exposure. 2011. p. 79650R

Perkins L, Hughes E, Srinivasan L, Allsop J, Glover A, Kumar S, Fisk N, Rutherford M. Exploring cortical subplate evolution using magnetic resonance imaging of the fetal brain. Dev. Neurosci. 2008; 30:211–220. [PubMed: 18075267]

Prastawa M, Gilmore JH, Lin W, Gerig G. Automatic segmentation of MR images of the developing newborn brain. Med. Image Anal. 2005; 9:457–466. [PubMed: 16019252]

Prayer D, Kasprian G, Krampl E, Ulm B, Witzani L, Prayer L, Brugger PC. MRI of normal fetal brain development. Eur. J. Radiol. 2006; 57:199–216. [PubMed: 16413984]

Prayer, D.; Brugger, PC.; Nemec, U.; Milos, RI.; Mitter, C.; Kasprian, G. Cerebral malformations. In: Prayer, D., editor. Fetal MRI. Springer; Berlin Heidelberg: 2011. p. 287-308.

Pugash, D.; Nemec, U.; Brugger, PC.; Prayer, D. Fetal MRI of normal brain development. In: Prayer, D., editor. Fetal MRI. Springer; Berlin Heidelberg: 2011. p. 147-175.

Rados M, Judas M, Kostovic I. In vitro MRI of brain development. Eur. J. Radiol. 2006; 57:187–198. [PubMed: 16439088]

Rajagopalan V, Scott J, Habas PA, Kim K, Rousseau F, Glenn OA, Barkovich AJ, Studholme C. Mapping directionality specific volume changes using tensor based morphometry: an application to the study of gyrogenesis and lateralization of the human fetal brain. Neuroimage. 2012; 63:947–958. [PubMed: 22503938]

Rutherford M, Jiang S, Allsop J, Perkins L, Srinivasan L, Hayat T, Kumar S, Hajnal J. MR imaging methods for assessing fetal brain development. Dev. Neurobiol. 2008; 68:700–711. [PubMed: 18383541]

Sbarbati A, Marzola P, Simonati A, Nicolato E, Osculati F. High-field magnetic resonance imaging of the developing human brain from the 10th to the 16th week of gestational age. Acta Anat. (Basel). 1998; 163:39–46. [PubMed: 9852353]

Scott JA, Habas PA, Kim K, Rajagopalan V, Hamzelou KS, Corbett-Detig JM, Barkovich AJ, Glenn OA, Studholme C. Growth trajectories of the human fetal brain tissues estimated from 3D reconstructed in utero MRI. Int. J. Dev. Neurosci. 2011; 29:529–536. [PubMed: 21530634]

Scott JA, Habas PA, Rajagopalan V, Kim K, Barkovich AJ, Glenn OA, Studholme C. Volumetric and surface-based 3D MRI analyses of fetal isolated mild ventriculomegaly: brain morphometry in ventriculomegaly. Brain Struct. Funct. 2012:1–11.

Serag A, Aljabar P, Ball G, Counsell SJ, Boardman JP, Rutherford MA, Edwards AD, Hajnal JV, Rueckert D. Construction of a consistent high-definition spatio-temporal atlas of the developing brain using adaptive kernel regression. Neuroimage. 2012; 59:2255–2265. [PubMed: 21985910]

Sethian JA. A fast marching level set method for monotonically advancing fronts. Proc. Natl. Acad. Sci. U. S. A. 1996; 93:1591–1595. [PubMed: 11607632]

Shattuck D, Leahy R. BrainSuite: an automated cortical surface identification tool. Medical Image Computing and Computer-Assisted Intervention — MICCAI 2000. Lect. Notes Comput. Sci. 2000:50–61.

Shattuck DW, Leahy RM. BrainSuite: an automated cortical surface identification tool. Med. Image Anal. 2002; 6:129–142. [PubMed: 12045000]

Shattuck DW, Mirza M, Adisetiyo V, Hojatkashani C, Salamon G, Narr KL, Poldrack RA, Bilder RM, Toga AW. Construction of a 3D probabilistic atlas of human cortical structures. Neuroimage. 2008; 39:1064–1080. [PubMed: 18037310]

Sled JG, Zijdenbos AP, Evans AC. A nonparametric method for automatic correction of intensity nonuniformity in MRI data. IEEE Trans. Med. Imaging. 1998; 17:87–97. [PubMed: 9617910]

Smith SM. Fast robust automated brain extraction. Hum. Brain Mapp. 2002; 17:143–155. [PubMed: 12391568]

Sowell ER, Leow AD, Bookheimer SY, Smith LM, O'Connor MJ, Kan E, Rosso C, Houston S, Dinov ID, Thompson PM. Differentiating prenatal exposure to methamphetamine and alcohol versus alcohol and not methamphetamine using tensor-based brain morphometry and discriminant analysis. J. Neurosci. 2010; 30:3876. [PubMed: 20237258]

Stein JL, Hua X, Lee S, Ho AJ, Leow AD, Toga AW, Saykin AJ, Shen L, Foroud T, Pankratz N. Voxelwise genome-wide association study (vGWAS). Neuroimage. 2010; 53(3):1160. [PubMed: 20171287]

Sundar H, Silver D, Gagvani N, Dickinson S. Skeleton based shape matching and retrieval. IEEE. 2003:130–139.

Sur M, Rubenstein JL. Patterning and plasticity of the cerebral cortex. Science. 2005; 310:805–810. [PubMed: 16272112]

Toro R, Burnod Y. A morphogenetic model for the development of cortical convolutions. Cereb. Cortex. 2005; 15:1900–1913. [PubMed: 15758198]

Twickler DM, Magee KP, Caire J, Zaretsky M, Fleckenstein JL, Ramus RM. Second-opinion magnetic resonance imaging for suspected fetal central nervous system abnormalities. Am. J. Obstet. Gynecol. 2003; 188:492–496. [PubMed: 12592261]

Van Essen DC. A tension-based theory of morphogenesis and compact wiring in the central nervous system. Nature. 1997; 385:313–318. [PubMed: 9002514]

Weisenfeld NI, Warfield SK. Automatic segmentation of newborn brain MRI. Neuroimage. 2009; 47:564–572. [PubMed: 19409502]

Xue H, Srinivasan L, Jiang S, Rutherford M, Edwards AD, Rueckert D, Hajnal JV. Automatic segmentation and reconstruction of the cortex from neonatal MRI. Neuroimage. 2007; 38:461–477. [PubMed: 17888685]

Yang Y, Raine A. Prefrontal structural and functional brain imaging findings in antisocial, violent, and psychopathic individuals: a meta-analysis. Psychiatry Res. 2009; 174:81–88. [PubMed: 19833485]

Yoon U, Fonov VS, Perusse D, Evans AC. The effect of template choice on morphometric analysis of pediatric brain data. Neuroimage. 2009; 45:769–777. [PubMed: 19167509]

Zhang Z, Liu S, Lin X, Sun B, Yu T, Geng H. Development of fetal cerebral cortex: assessment of the folding conditions with post-mortem magnetic resonance imaging. Int. J. Dev. Neurosci. 2010; 28:537–543. [PubMed: 20457247]

Zhang Z, Liu S, Lin X, Teng G, Yu T, Fang F, Zang F. Development of fetal brain of 20 weeks gestational age: assessment with post-mortem magnetic resonance imaging. Eur. J. Radiol. 2011a; 80:e432–e439. [PubMed: 21146341]

Zhang Z, Liu S, Lin X, Teng G, Yu T, Fang F, Zang F. Development of laminar organization of the fetal cerebrum at 3.0 T and 7.0 T: a postmortem MRI study. Neuroradiology. 2011b; 53:177–184. [PubMed: 20981415]

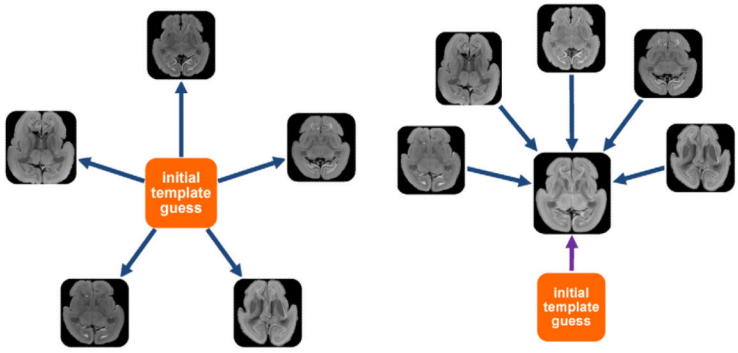

Fig. 1.

Building average fetal templates. Using the data at 19th GW as an example, we illustrate the two steps in our optimization of a population template through asymmetric diffeomorphic parameterization. *Left*: the shape of an initial template guess (orange cube) is updated by first estimating the diffeomorphic paths (blue arrow). *Right*: we then change the diffeomorphism representing the initial conditions of each diffeomorphic path and each pairwise problem is solved with SyN (purple arrow), to map between the template and the individual images, to shorten their total length. In this 2-step process, the template shape also changes under the initial conditions (purple arrow).

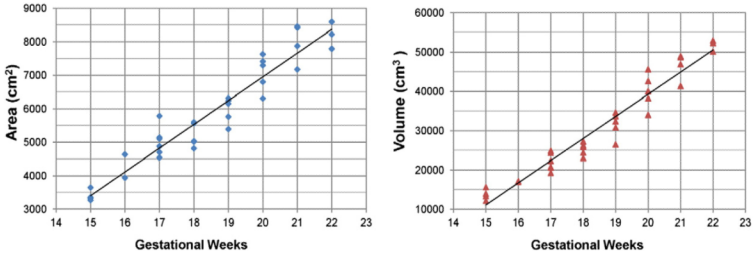

Fig. 2.

Linear growth estimates for area and volume of fetal brain from 15 to 22 GW. Both area (left) and volume (right) significantly increase linearly. Correlation (GW, Area) = 0.958, R^2 = .919, correlation (GW, Volume) = 0.970, R^2 = .940.

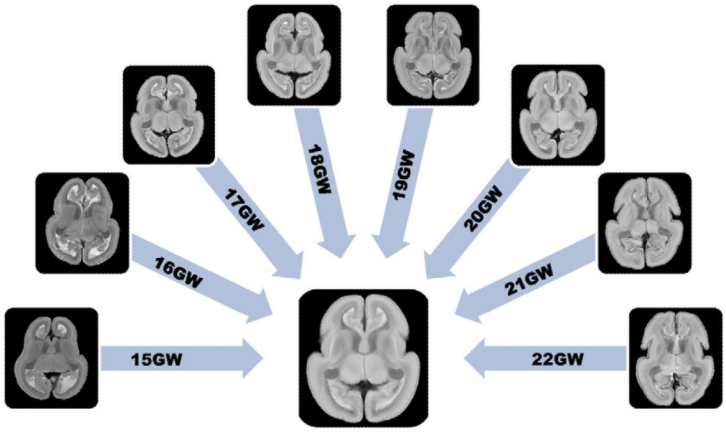

Fig. 3.

Schematic of the protocol for construction of the Fetal Brain Atlas of the early second trimester. The image sections around the template represent the corresponding weekly templates (see Fig. 1).

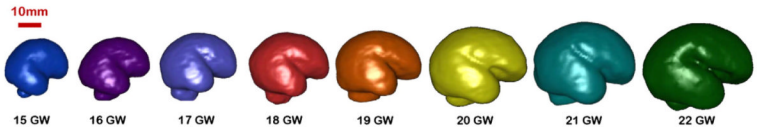

Fig. 4.
Cortical surface models based on the weekly brain templates for each GW.

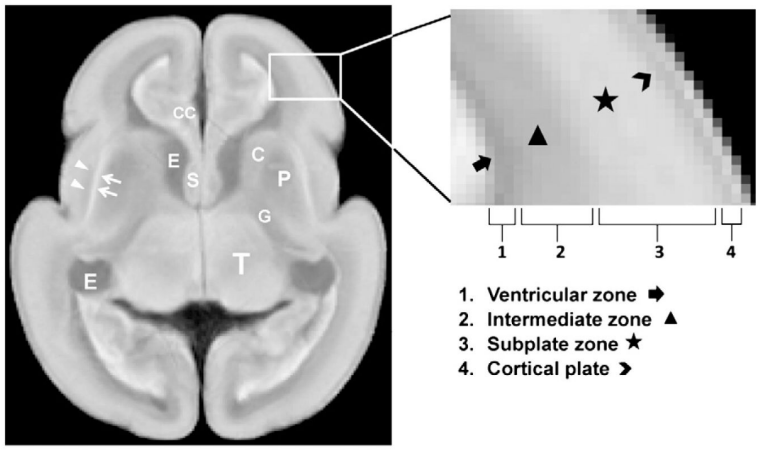

Fig. 5.

An axial view of the template with an average shape and intensity MR T2W image. One piece of the cerebral wall is enlarged to show the lamination organization in details. The annotation of each layer is shown at the right bottom. Abbreviations in the template view: P, putamen; C, caudate nucleus; T, thalamus; E, ganglionic eminence; CC, corpus callosum; S, septum; G, globus pallidus; double arrows, external capsule; double arrow heads, claustrum.

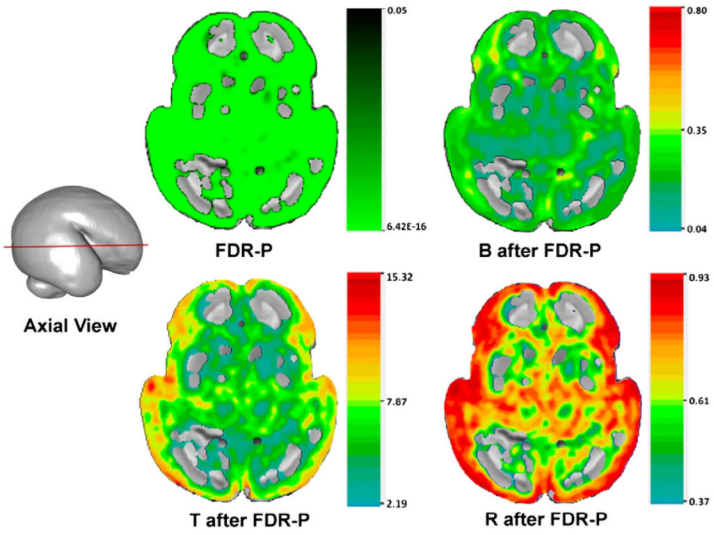

Fig. 6.

Linear modeling of the effects of GW on the TBM maps. Maps of FDR-corrected (P = 0.05) P-values, effect-sizes (B) and correlations (T and R) are shown. These results indicate that the cortex has a relatively bigger growth rate and higher correlation compared with the subcortex, especially in the subplate zone.

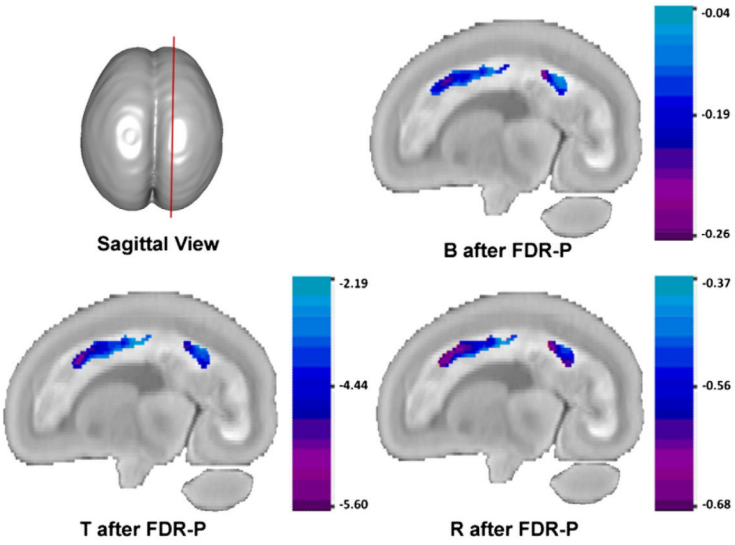

Fig. 7.

Linear modeling of GW effects on the lateral ventricles. Maps of negative effect-sizes (B) and correlations (T and R) (following FDR-correction for multiple testing) reveal shrinking morphometric changes in the lateral ventricle relative to the overall size of the brain, especially in the area of the frontal and parietal lobes.

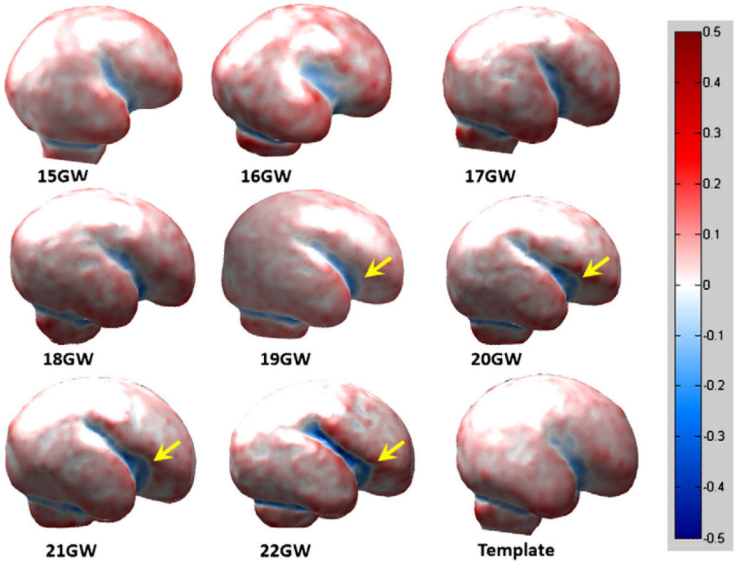

Fig. 8.

3D cortical surface curvature. These surface models represent the corresponding gestational week's templates. The cortical model in the lower right corner represents the overall template spanning the entire 8-week period. The surfaces have been manually adjusted to the same size and are not displayed with the same spatial scale. The yellow arrow represents the circular sulcus. Hot colors with positive values represent convex and cool colors with negative values represent concave.

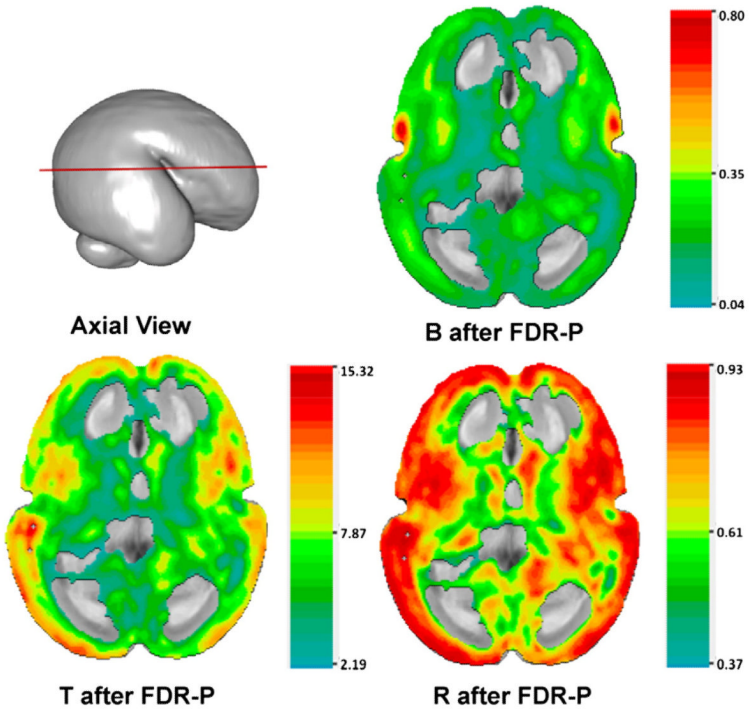

Fig. 9.

Linear modeling of the GW effects on the Sylvian fissure. Cortex around the Sylvian fissure showed higher B, T and R values (following FDR-correction), which implies bigger growth rate and higher correlation with GW. Changes in the cortex surrounding the Sylvian fissure are related to the formation of the Sylvian fissure.

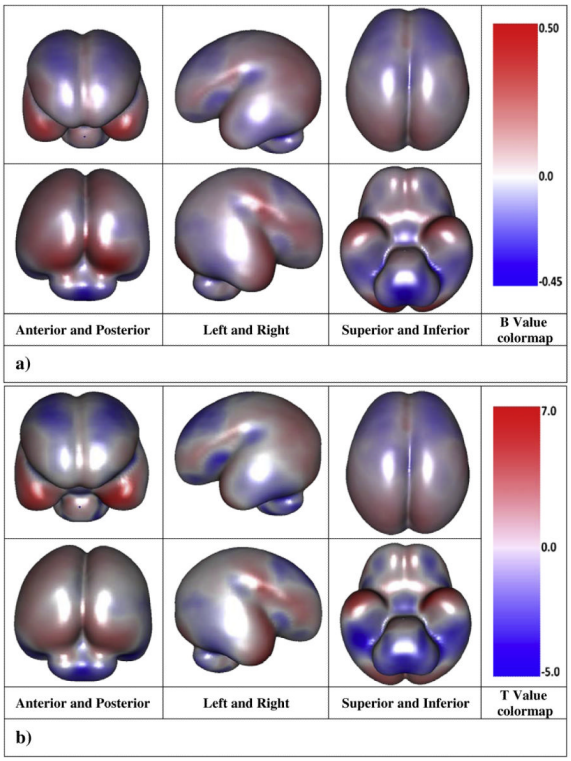

Fig. 10.

a: Age-related effect sizes of local displacement-field shown in 6 views. Red and blue colors represent positive and negative B values (effect-sizes), respectively. b: Local displacement-field analysis of the fetal brain surface in 6 views. Correlation maps between displacement-field changes and GW expressed by T maps. Red and blue colors represent positive and negative T values, respectively.

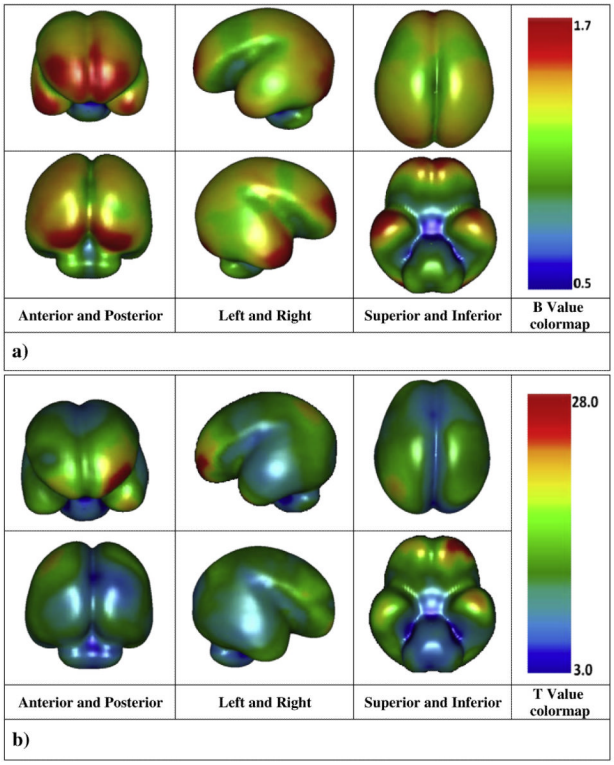

Fig. 11.

a: Age-related effect size of GW on localized radial-distance changes shown in 6 views. Hot and cold colors represent larger or smaller B values, respectively. b: Correlation T-value maps between GW and local radial-distance (as a proxy measure of fetal brain growth) in 6 cortical surface views. Hot and cold colors represent larger (more significant) correlations, respectively.

Table 1

Demographic distributions of the specimens.

GW	Number (total 34)	Gender (M:F)	Head circumference (cm)	Crown–rump length (cm)	Foot length (cm)	Abortion reasons
15	4	1:3	11.3 ± 0.54	10.8 ± 0.68	1.8 ± 0.08	SA(2), TI, UNK
16	2	2:0	13.1 ± 0.14	11.5 ± 0.00	2.1 ± 0.04	SA, SIC
17	6	2:4	14.2 ± 0.50	13.4 ± 0.37	2.4 ± 0.16	SA(2), SIC, TI, UNK(2)
18	5	3:2	15.4 ± 1.25	14.1 ± 1.57	2.6 ± 0.19	SA(2), TI, UNK(2)
19	5	3:2	15.9 ± 0.92	15.5 ± 0.71	2.9 ± 0.19	SA(2), SIC(2), FCA
20	5	1:4	17.1 ± 0.85	16.6 ± 0.85	3.1 ± 0.09	SA(3), SIC, UNK
21	4	0:4	18.6 ± 1.00	17.0 ± 0.49	3.2 ± 0.22	SA, SIC(2), UNK
22	3	0:3	19.2 ± 0.82	18.8 ± 0.87	3.6 ± 0.14	FCA, SIC, UNK

Abbreviations in the table: M, male; F, female; FCA, fetal chromosomal abnormality; TI, teratogenesis infection; SA, spontaneous abortion; SIC, stressful intrauterine conditions; UNK, unknown reasons of malformation (not brain) detected by US or MRI.